



UNIVERSITY OF LEEDS

This is a repository copy of *Gain-of-Function Genetic Alterations of G9a Drive Oncogenesis*.

White Rose Research Online URL for this paper:
<http://eprints.whiterose.ac.uk/169682/>

Version: Accepted Version

Article:

Kato, S, Weng, QY, Insko, ML et al. (20 more authors) (2020) Gain-of-Function Genetic Alterations of G9a Drive Oncogenesis. *Cancer Discovery*, 10 (7). pp. 980-997. ISSN 2159-8274

<https://doi.org/10.1158/2159-8290.cd-19-0532>

©2020 American Association for Cancer Research. This is an author produced version of an article published in *Cancer Discovery*. Uploaded in accordance with the publisher's self-archiving policy.

Reuse

Items deposited in White Rose Research Online are protected by copyright, with all rights reserved unless indicated otherwise. They may be downloaded and/or printed for private study, or other acts as permitted by national copyright laws. The publisher or other rights holders may allow further reproduction and re-use of the full text version. This is indicated by the licence information on the White Rose Research Online record for the item.

Takedown

If you consider content in White Rose Research Online to be in breach of UK law, please notify us by emailing eprints@whiterose.ac.uk including the URL of the record and the reason for the withdrawal request.



eprints@whiterose.ac.uk
<https://eprints.whiterose.ac.uk/>

Supplementary Figures and legends

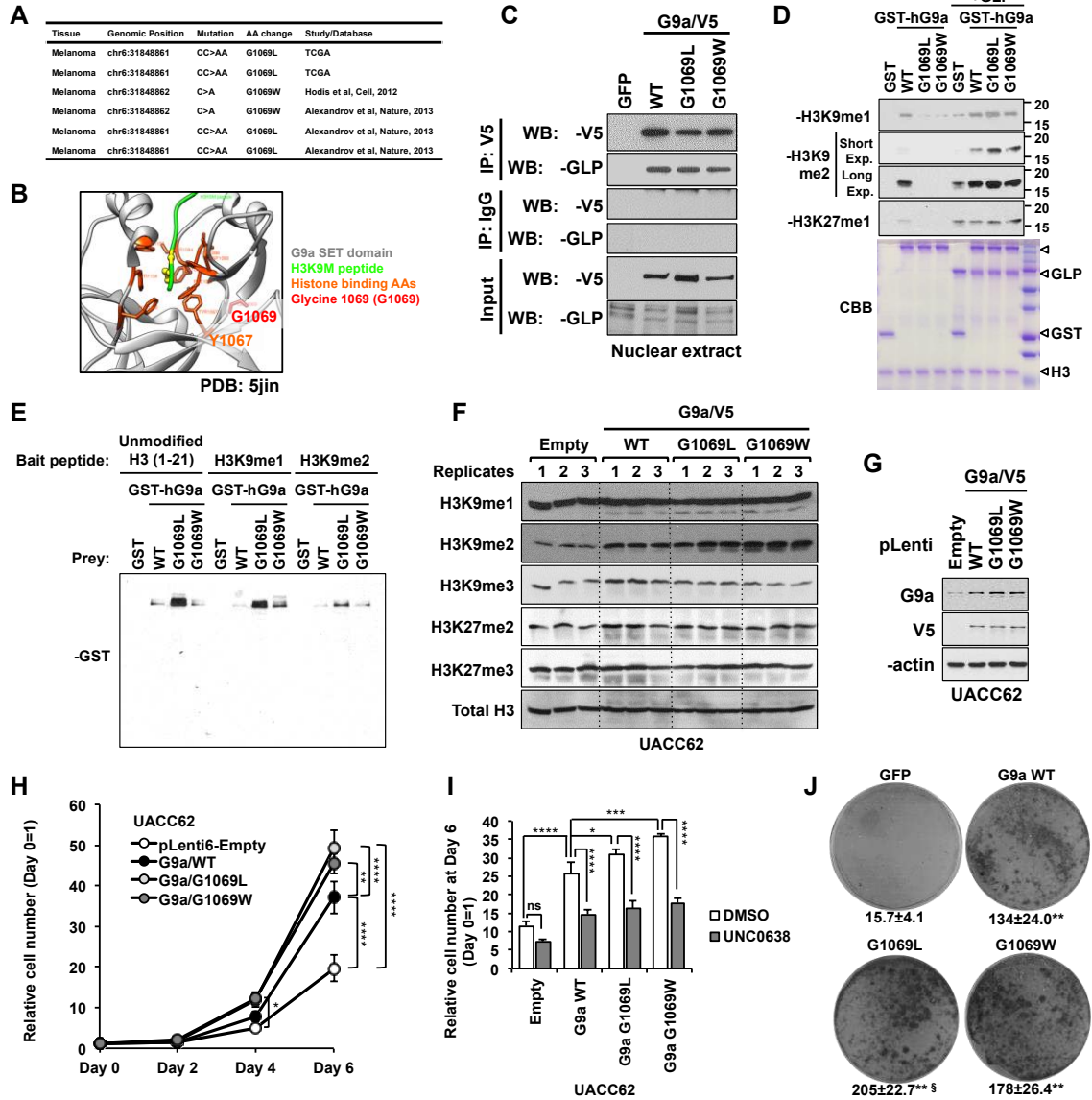
Supplementary Figure S1. Effects of G1069L and G1069W mutations on methyltransferase activity of G9a *in vitro* (Related to Figure 1).

(A) List of human melanomas with a G1069L/W mutation and the source database/study. **(B)** Co-crystalized structure of G9a and H3K9M mutant peptide obtained from the Protein Data Bank (PDB: 5jin). A part of the co-crystalized structure was visualized by JSmol. G1069 is located immediately adjacent to the highly conserved catalytic site, Y1067, and other histone-binding amino acids. **(C)** Co-immunoprecipitation of V5-tagged G9a (G9a/V5) and GLP in 293T cells. 24 h after transfection of either G9a wild type (WT) or mutants, nuclear protein fractions were extracted and subsequently used for co-immunoprecipitation using anti-V5 antibody. **(D)** *In vitro* methyltransferase assay using GST-fused recombinant G9a and recombinant human H3 protein. Briefly, 2 μ g of H3 protein was incubated with 2 μ g of either GST, GST-G9a, GST-G9a G1069L, or GST-G9a G1069W, with or without 1 μ g of recombinant GLP, in the presence of 2 μ M S-adenosyl methionine (SAM) for 1h at RT. Subsequently, the mixture was subjected to western blotting using specific anti-methyl H3 antibodies. Coomassie Brilliant Blue (CBB) staining was used as an internal control to ensure similar amounts of the recombinant proteins. **(E)** Pull-down assay for recombinant human G9a and histone H3 peptides. After elution, histone H3-interacting GST-G9a WT and mutant proteins were visualized by immunoblot using anti-GST antibody. **(F)** Western blots of global H3K9 mono-, di-, and tri-methylation levels and H3K27 di- and tri-methylation levels in G9a WT-, G1069L-

, and G1069W-overexpressing UACC62 melanoma cells. **(G)** Western blot of G9a/V5 WT and G1069 mutants in the overexpressing UACC62 cells of F. **(H)** Effects of G9a WT, G1069L, and G1069W on UACC62 proliferation. Cell numbers were manually counted by trypan blue exclusion assay. ** $p < 0.01$, **** $p < 0.0001$ by repeated measures two-way ANOVA of 3 replicates with the Holm-Šidák correction for multiple pairwise comparisons of the four groups at each time point. **(I)** Effects of G9a/GLP inhibitor UNC0638 on the enhanced proliferation of G9a WT-, G1069L-, and G1069W-expressing UACC62 cells. The cells were cultured in the presence of 1 μM UNC0638 for 6 days. Cell numbers were counted manually and normalized to Day 0. * $p < 0.05$, *** $p < 0.001$, **** $p < 0.0001$ by regular two-way ANOVA of 3 replicates with the Holm-Šidák correction for multiple pairwise comparisons. **(J)** Transformation assay of G9a and oncogenic G1069L/W mutants in NIH3T3 cells. Following infection with the indicated gene, NIH3T3 cells were cultured for 10 days without blasticidin selection. Representative images from one of two independent experiments are shown and average colony numbers \pm SD of 3-4 replicates are indicated below the images. ** $p < 0.01$ vs. GFP, § $p < 0.05$ vs. G9a WT by one-way ANOVA with the Holm-Šidák correction for multiple pairwise comparisons.

Supplementary Figure S1.

Figure S1

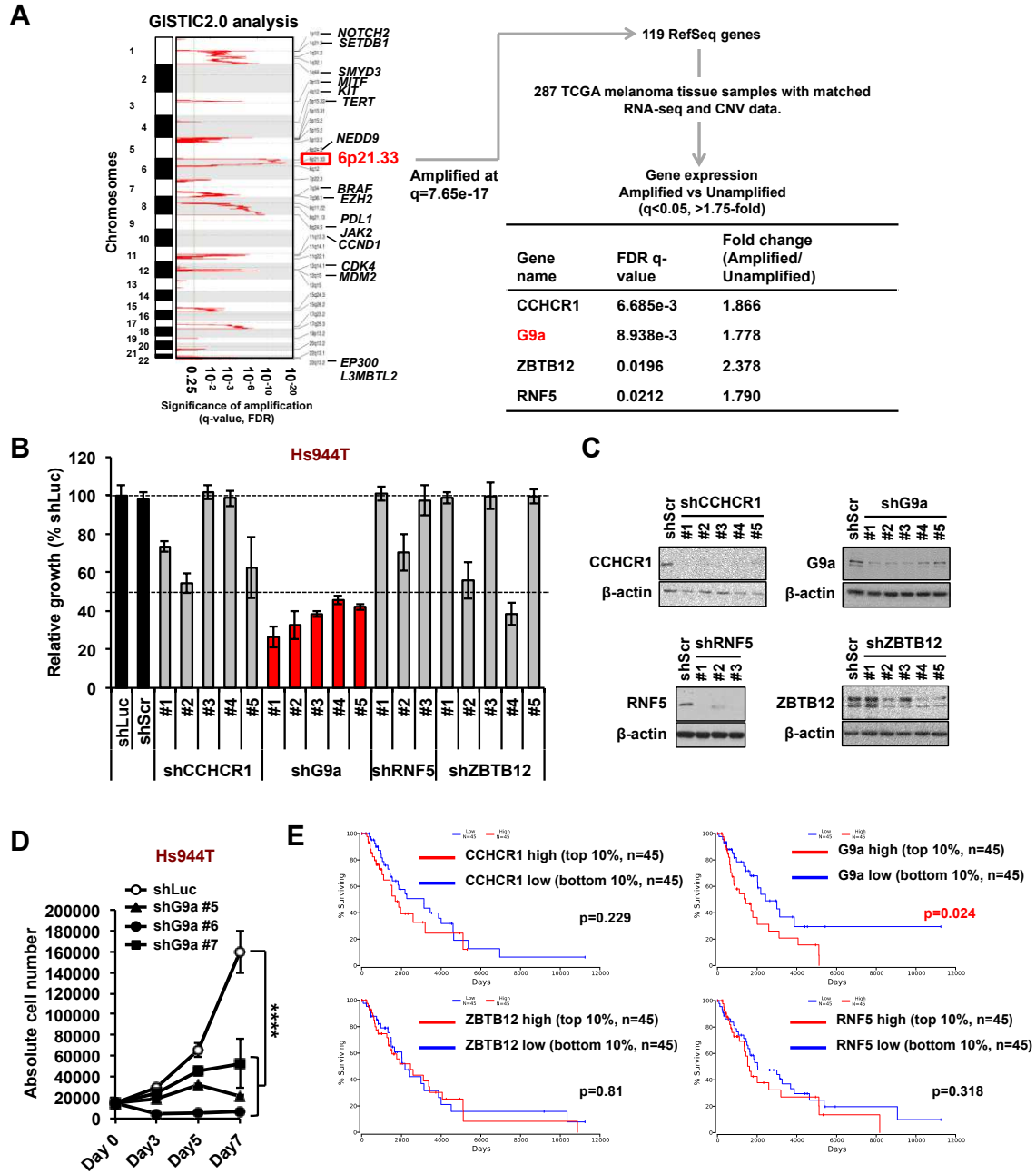


Supplementary Figure S2. *G9a* is a candidate oncogene in 6p21-gained melanomas (Related to Figure 2).

(A) Schema of the approach for identification of oncogenes located on chromosome 6p21. 505 TCGA melanoma cases with copy number data were analyzed by GISTIC2.0, from which 287 cases with both SNP array and RNA-seq analysis were filtered for higher expression in 6p21-amplified vs. non-amplified melanomas (FDR $q < 0.05$ and fold change > 1.75). **(B)** Dependence of 6p21-amplified melanoma cell line Hs944T on *G9a*, but not on other candidate genes located in the 6p21 amplicon. Hs944T cells were infected with 3-5 different shRNA hairpins targeting *G9a* or the other candidate genes (*CCHCR1*, *RNF5*, *ZBTB12*). Equal numbers of infected cells were re-seeded in 24-well plates and further cultured for 7 days to assess colony formation, which is normalized to the shLuc control. Data represent mean \pm SD of three independent experiments. **(C)** Western blots showing knockdown efficiencies of the shRNAs used in the assay of Figure S2B. Representative images from two independent experiments are shown. **(D)** Proliferation of Hs944T cells following stable shRNA-mediated *G9a* knockdown. Equal numbers of Hs944T cells infected with the different shRNAs were re-seeded after puromycin selection and the cell number was quantified by cell counting at the indicated time points. **(E)** Kaplan-Meier survival plots of TCGA melanoma patients. 450 TCGA melanomas were ordered according to mRNA expression level of *CCHCR1* (top, left), *G9a* (top, right), *ZBTB12* (bottom, left) or *RNF5* (bottom, right) and linked with patient survival

data. The 10% of patients with the highest and lowest intratumoral levels of the indicated mRNAs are shown.

Supplementary Figure S2.



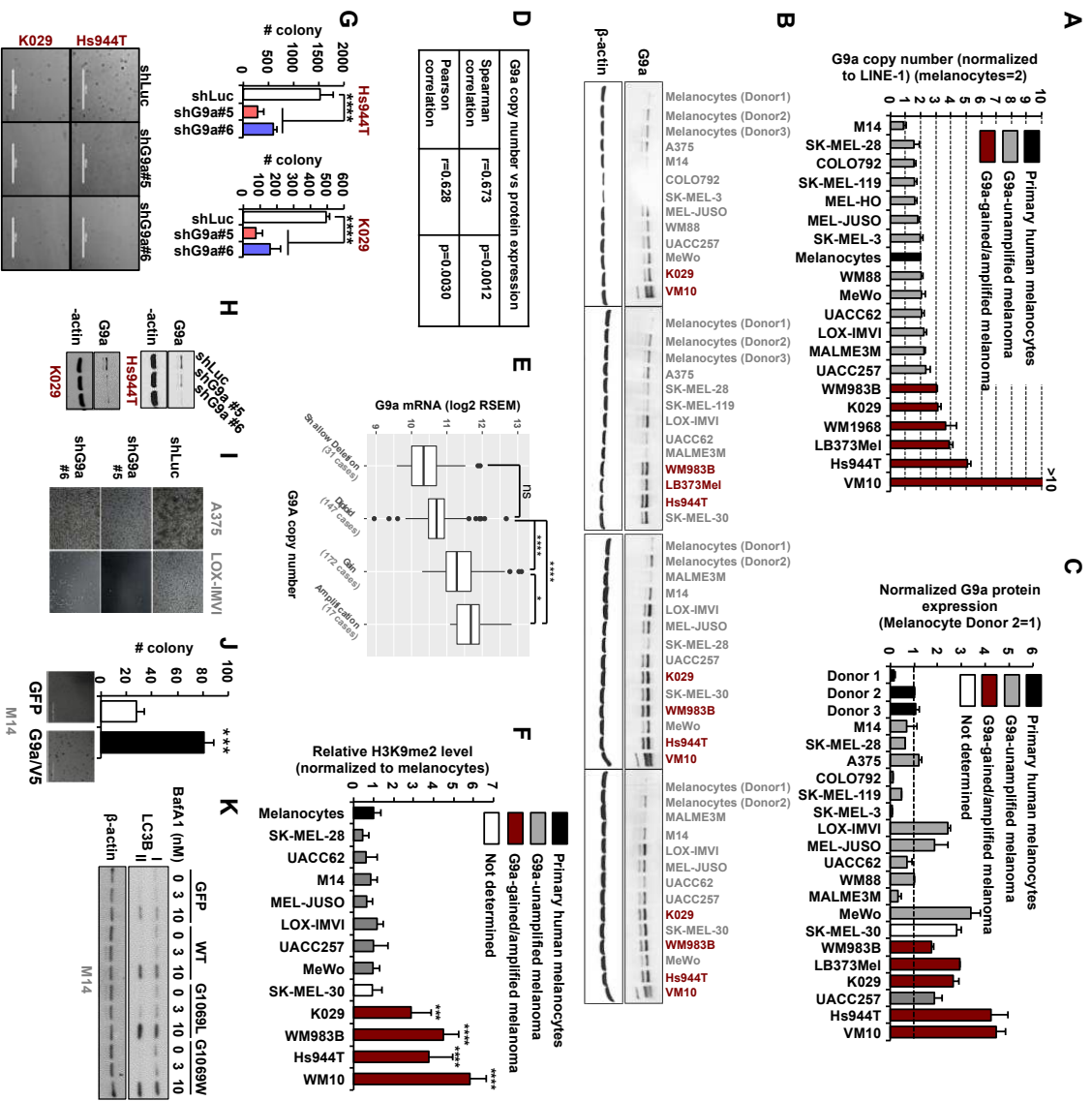
Supplementary Figure S3. *G9a* copy number gains correlate with high *G9a* protein and mRNA levels, H3K9me2 levels, and susceptibility to *G9a* inhibition (Related to Fig. 2).

(A) Quantification of *G9a* copy number in melanoma cell lines and primary human melanocytes by genomic qPCR. *G9a* copy number was measured using primer pairs targeting the 3'UTR of *G9a*. **(B)** Western blot images of *G9a* across human melanoma cell lines and primary human melanocytes. *G9a*-gained/amplified melanoma cell lines are labeled in red. **(C)** Quantified *G9a* protein expression normalized to β -actin expression from the western blots. Data represent mean \pm SD normalized intensity from two-three independent experiments. **(D)** Spearman and Pearson correlation coefficients between *G9a* copy number and *G9a* protein expression. **(E)** Association of *G9a* copy number with mRNA expression level in the TCGA melanoma dataset. * $p < 0.05$, **** $p < 0.00001$ by one-way ANOVA with the Holm-Šidák correction for multiple pairwise comparisons. **(F)** Quantified H3K9me2 levels relative to total histone H3 levels in primary human melanocytes and melanoma cell lines from the western blots in Fig. 2C. The values in the melanoma lines are normalized to primary melanocytes. Data represent mean \pm SD normalized intensity of 4 independent experiments. *** $p < 0.001$, **** $p < 0.0001$ compared with melanocytes by one-way ANOVA with the Holm-Šidák correction for multiple pairwise comparisons. **(G)** Soft agar assay in *G9a*-amplified/H3K9me2-high melanoma cell lines with *G9a* knockdown. **** $p < 0.0001$ compared with shLuc by two-way ANOVA with the Holm-Šidák correction for multiple pairwise comparisons. **(H)** Knockdown

efficiency of shG9a hairpins in *G9a*-amplified/H3K9me2-high melanoma cell lines, Hs944T and K029. **(I)** Macroscopic cellular images 7 days after shControl or shG9a infection in A375 or LOX-IMVI cells. **(J)** Soft agar assay of M14 cells overexpressing G9a/V5 or GFP (control). Data with error bars represent mean \pm SD of 6 replicates. *** $p < 0.001$ by unpaired, two-tailed T test. **(K)** Western blots of LC3B in M14 cells overexpressing GFP control, G9a wild type (WT) or G1069L/W mutants after treatment with bafilomycin A1 (BafA1) or DMSO vehicle for 24 h. Representative images from two independent experiments are shown.

Supplementary Figure S3.

Figure S3



Supplementary Figure S4. Therapeutic impact of potent G9a inhibitor UNC0642 in preclinical xenograft mouse model. (Related to Fig. 2)

(A) Tumor weights and images of K029 xenografts in nude mice treated daily with vehicle (10% DMSO/PBS) or UNC0642 (2.5 mg/kg) for 17 days. n=5 mice/group, analyzed by unpaired, two-tailed T test. **(B)** Body weights of K029 tumor-bearing nude mice treated daily with vehicle or UNC0642 for 17 days. **(C and D)** Growth of individual Hs944T xenograft tumors in mice treated daily with vehicle (10% DMSO/PBS) (J) or UNC0642 (2.5 mg/kg) (K). Red lines (2/8) indicate complete tumor regressions. **(E)** Kaplan-Meier survival curves of Hs944T-xenografted mice treated with vehicle (10% DMSO/PBS, control) or UNC0642 (2.5 mg/kg). n=5 mice/group, analyzed by the log-rank (Mantel-Cox) test. **(F)** Western blots of BRAF^{V600E}-expressing pMEL* (pMEL*BRAF(V600E)) cells overexpressing G9a/V5 or GFP (control), showing DKK1, active β -catenin, MITF, and H3K9me2 levels. **(G)** Soft agar assay of pMEL*/BRAF(V600E) cells overexpressing GFP (control) or G9a/V5. Black- and white-filled columns indicate large (>20 mm) and small colonies, respectively. Representative images are shown below the graph. Large colonies: **p<0.01 vs. GFP; small colonies: ***p<0.001 vs. GFP by unpaired, two-tailed T-test. **(H)** Melanoma free survival curves of mice carrying xenografts of pMEL*/BRAF(V600E) cells overexpressing GFP or G9a/V5. n=10 mice/group, ***p<0.001 by the log-rank (Mantel-Cox) test. **(I)** Photo images of representative mice 28 days after inoculation of pMEL*/BRAF/GFP or pMEL*/BRAF/G9a cells and treatment with vehicle or UNC0642 as in K (below). **(J)** Macroscopic tumors excised from vehicle- or

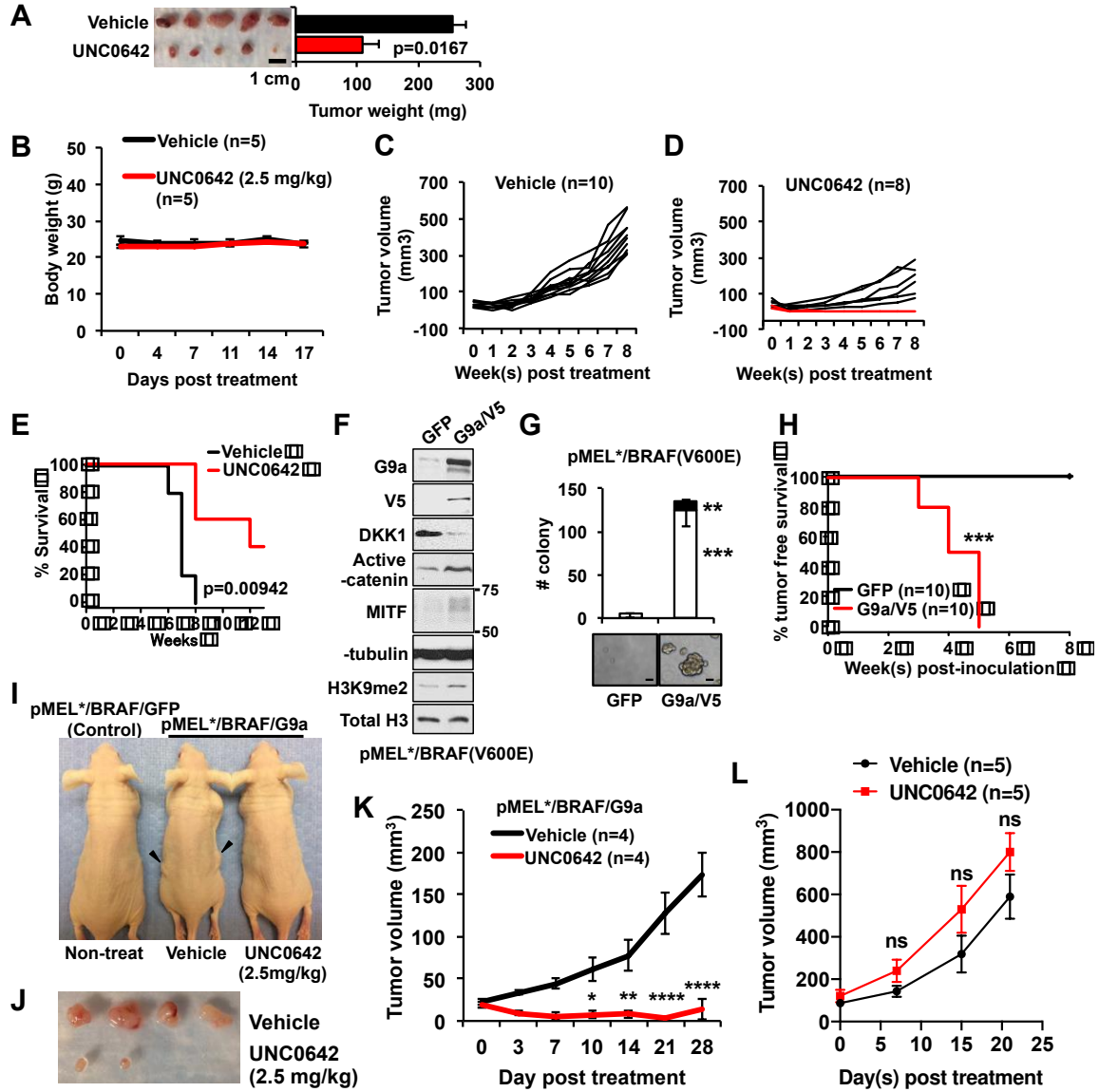
UNC0642-treated pMEL*/BRAF/G9a xenograft mice 28 days after inoculation.

Two of 4 UNC0642-treated tumors regressed completely in this xenograft model.

(K) Tumor growth curves of pMEL*/BRAF/G9a xenografts in mice treated with vehicle or UNC0642 (2.5 mg/kg). Mice were treated every other day for 28 days, beginning 8 weeks after inoculation of 1×10^6 pMEL*/BRAF/G9a cells. **(L)** Tumor growth curves of *G9a* diploid UACC62 melanoma cell xenografts in mice treated daily with vehicle (n=5) or UNC0642 (n=5) beginning 14 days after inoculation.

*p<0.05, **p<0.01, ****p<0.0001 by repeated measures two-way ANOVA with the Holm-Šidák correction for multiple pairwise comparisons of the two groups at each time point. Data represent mean \pm SEM (n=4).

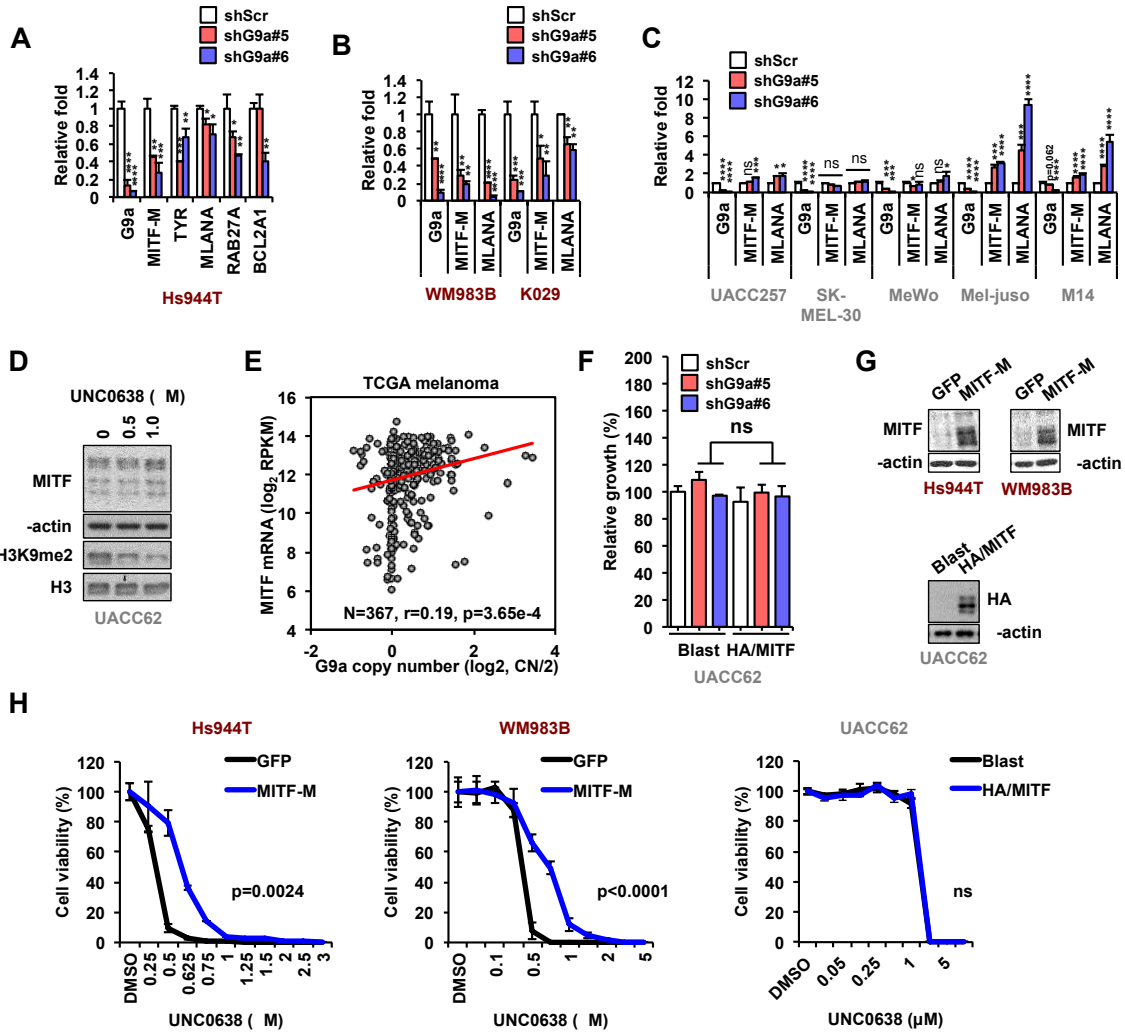
Supplementary Figure S4.



Supplementary Figure S5. G9a positively regulates MITF in G9a-gained/amplified melanoma cells (Related to Figure 3).

(A-C) qRT-PCR for MITF and target genes upon *G9a* knockdown in *G9a*-amplified melanoma cell line Hs944T (A); *G9a*-gained melanoma cell lines WM983B and K029 (B); and *G9a*-unamplified melanoma cell lines (C). * $p < 0.05$, ** $p < 0.01$, *** $p < 0.001$, **** $p < 0.0001$ by ordinary one-way ANOVA of 3 replicates with the Holm-Šidák correction for pairwise comparisons of *G9a* shRNAs to shScr, separately for each gene or cell line. **(D)** Western blots of MITF and H3K9me2 in *G9a* diploid UACC62 after UNC0638 treatment for 72h. Representative images from two independent experiments are shown. **(E)** Correlation between *G9a* copy number and *MITF* expression in TCGA patient melanomas (r = Pearson correlation coefficient; red line indicates the best fit by linear regression). **(F)** Minimal impact of *G9a* knockdown and MITF rescue on growth of UACC62 cells. **(G)** Western blots of MITF in melanoma cells expressing ectopic GFP or MITF. **(H)** GFP and MITF-overexpressing Hs944T (left), WM983B (middle), and UACC62 (right) cells were treated with UNC0638 for 72 h and cell viability was determined by CellTiter-Glo assay. Four replicates at each dose were analyzed by nonlinear regression (dose response-inhibition, variable slope) followed by unpaired, two-tailed T tests of the IC50s.

Supplementary Figure S5.

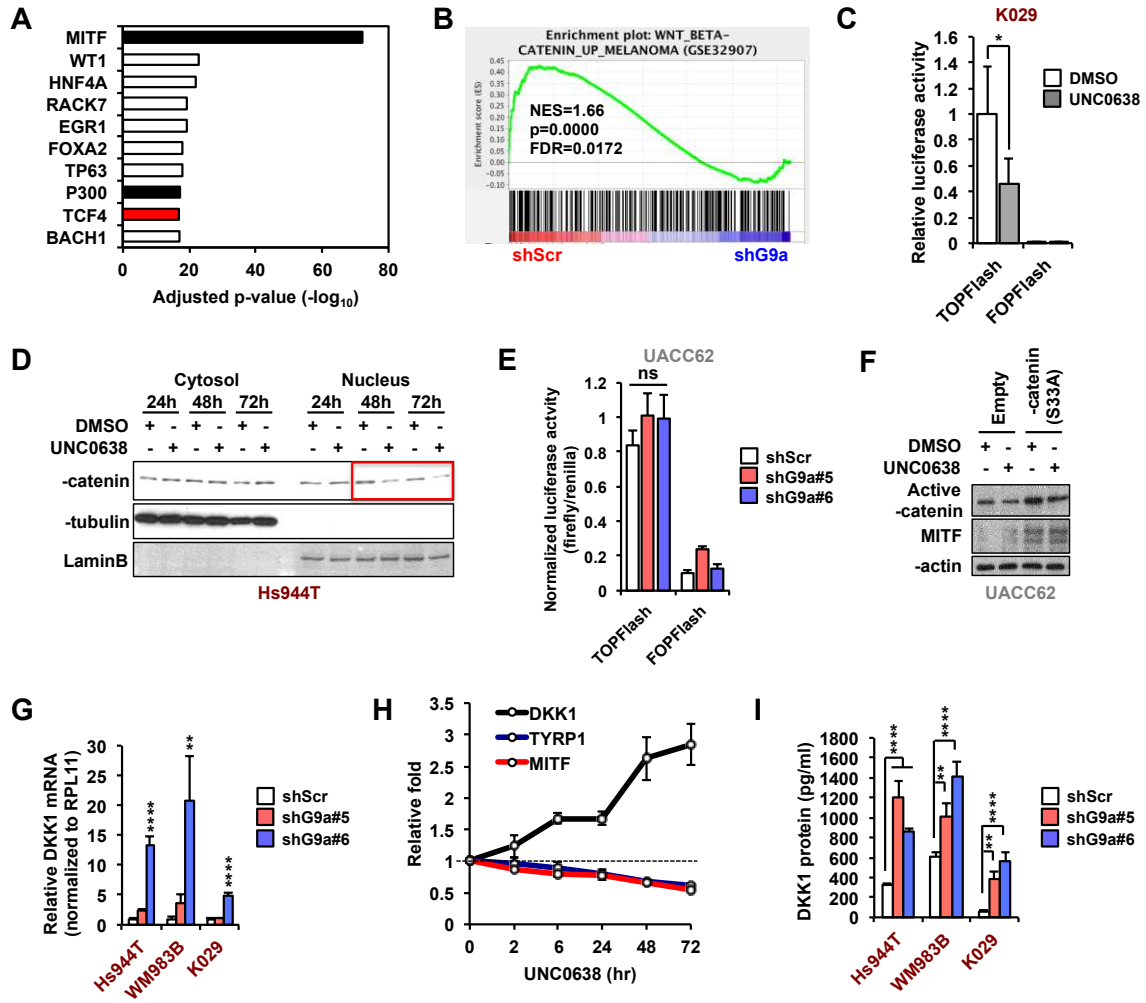


Supplementary Figure S6. G9a inhibition or knockdown induces the expression of WNT antagonist DKK1 and inactivates WNT/ β -catenin signaling (Related to Figures 3 and 4)

(A) Comprehensive gene set enrichment analysis using the Enrichr online platform with the ChEA (ChIP-X enrichment analysis) gene set library. The ChEA database enables reconstruction of a gene regulatory network of transcription factors and cofactors based on shared targets and proximity of binding sites (Lachmann A et al, Bioinformatics 26: 2438-44, 2010). The top 10 transcription factors/cofactors that are significantly enriched in the set of genes downregulated by *G9a* knockdown (283 genes, log₂ fold < -0.585, adjusted p-value < 0.05) in Hs944T melanoma cells are shown. **(B)** GSEA representation of the WNT/ β -catenin-upregulated target genes (WNT_BETA_CATENIN_UP_MELANOMA (GSE32907)) in whole transcriptome RNA-seq results of shG9a-treated vs. shScr control-treated Hs944T cells. **(C)** TOP/FOPFlash transcriptional activity following UNC0638 treatment for 48 h in *G9a*-gained K029 melanoma cells. FOPFlash is a control luciferase reporter with mutant TCF/LEF-binding sites. Data represents mean \pm SD of triplicates from three independent experiments, *p<0.05 by ratio paired T test. **(D)** Cytosolic and nuclear β -catenin expression in HS944T cells after treatment with UNC0638 (500 nM) for the indicated times. Red open square highlights suppression of nuclear β -catenin expression by UNC0638. **(E)** TOP/FOPFlash transcriptional activity following *G9a* knockdown for 72 h in *G9a* diploid UACC62 cells. Data represent the mean intensity \pm SD of two independent experiments. **(F)** Western blots of MITF and non-phosphorylated

(active) β -catenin in *G9a* diploid UACC62 melanoma cells expressing constitutively active β -catenin (S33A) or empty vector, after incubation with UNC0638 (750 nM) for 72 h. Representative images from two independent experiments are shown. **(G)** *DKK1* mRNA expression in *G9a*-amplified (Hs944T) and -gained (WM983B and K029) cells upon *G9a* knockdown. qRT-PCR was performed 72 h after shRNA infection and mRNA levels in *G9a* knockdown cells relative to levels in shScr control cells are shown. **(H)** Time courses of induction of *DKK1* mRNA and suppression of *MITF* and *TYRP1* (*MITF* target) mRNAs by UNC0638 (500 nM) in Hs944T cells. **(I)** ELISA for secreted *DKK1* levels 72 h after *G9a* knockdown in *G9a*-gained or -amplified melanoma cells. P-values in **G** and **I** were calculated by ordinary one-way ANOVA of 3 replicates with the Holm-Šidák correction for comparisons of *G9a* shRNAs to shScr, separately for each cell line. ** $p < 0.01$, **** $p < 0.0001$.

Supplementary Figure S6.



Supplementary Fig. S7. G9a overexpression represses DKK1 and induces MITF in G9a-unamplified melanomas. (Related to Fig. 4)

(A) Western blots of DKK1 and MITF in *G9a*-unamplified UACC62, MEL-JUSO, and SK-MEL-119 melanoma cells stably overexpressing G9a-V5 or GFP vector.

(B) ELISA for secreted DKK1 in G9a-V5 overexpressing and control UACC62 and SK-MEL-119 cells. *** $p < 0.001$, **** $p < 0.0001$ by unpaired, two-tailed T tests of 4 replicates with the Holm-Šidák correction for multiple comparisons. **(C)**

Macroscopic pigmentation difference in cell pellets of SK-MEL-119 cells overexpressing G9a-V5 or GFP vector. **(D)** qRT-PCR for DKK1, MITF, TRPM1 (MITF target), and CCND1 (WNT target) in *G9a*-unamplified melanoma cell lines overexpressing G9a-V5 or GFP vector. * $p < 0.05$, *** $p < 0.001$, **** $p < 0.0001$ by unpaired, two-tailed T tests of 3 replicates. No correction for multiple

comparisons was performed, as the effects of G9a on the different genes are not independent. **(E)** Western blots of M14 cells overexpressing G9a/V5 or GFP

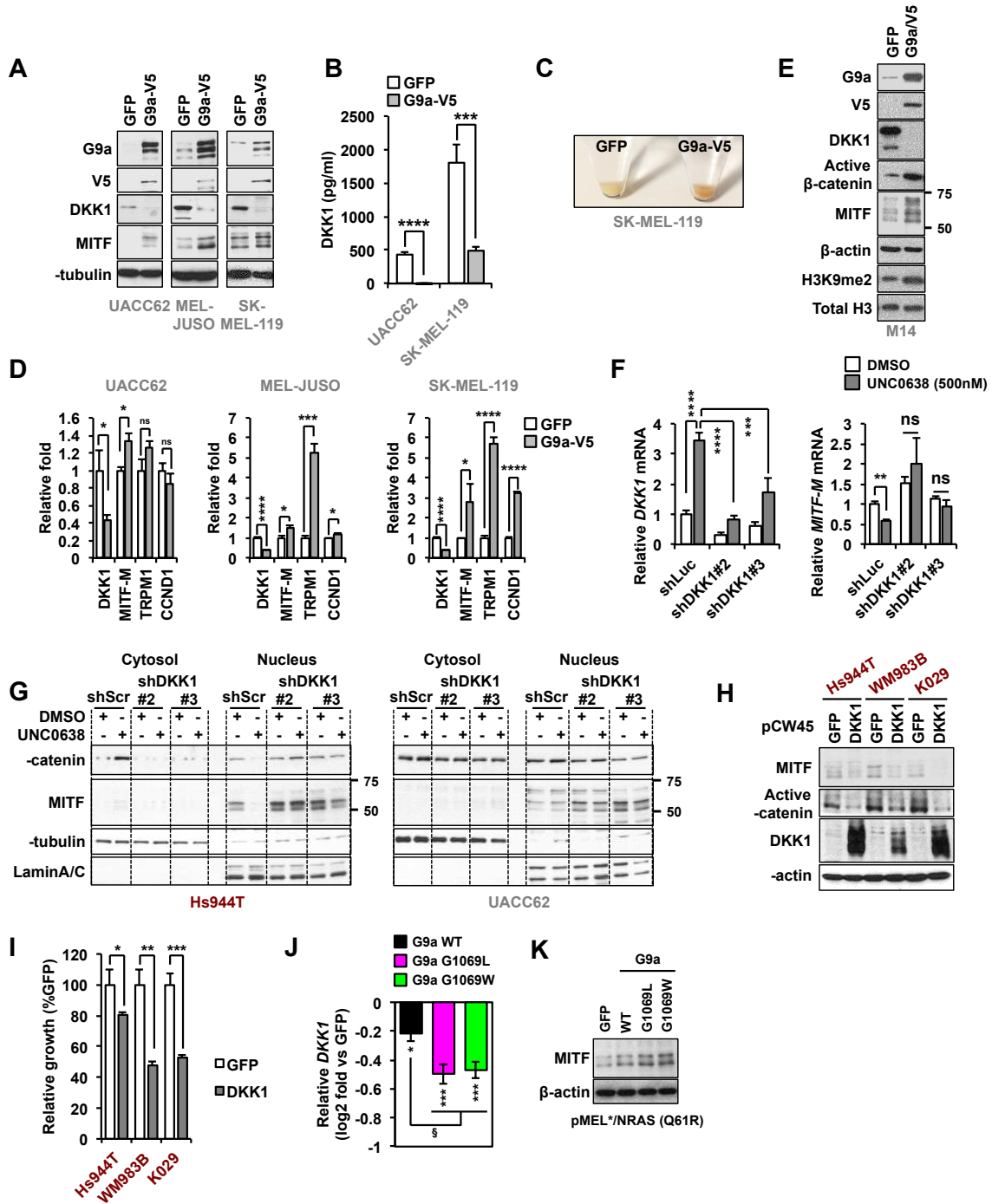
(control), showing DKK1, active β -catenin, MITF, and H3K9me2 levels. **(F)** Effect of *DKK1* knockdown on UNC0638-induced downregulation of *MITF* in WM983B cells. qRT-PCR for *DKK1* and *MITF-M* was performed in WM983B cells stably expressing shDKK1 or shLuc (control) hairpins, after incubation with UNC0638 (500 nM) or DMSO vehicle for 72h. Data represents mean \pm SD of three-

independent experiments. ** $p < 0.01$, *** $p < 0.01$, **** $p < 0.0001$ by two-way ANOVA (for *DKK1*) or multiple T tests (for *MITF-M*) with the Holm-Šidák correction for the

indicated pairwise comparisons. **(G)** Western blots of cytosolic and nuclear β -catenin and MITF expression in Hs944T (left) and UACC62 (right) cells

transduced with shScr or shDKK1 and treated with UNC0638 or DMSO vehicle. α -tubulin and LaminA/C served as internal controls for the cytosolic and nuclear fractions, respectively. **(H)** Western blots of DKK1, active β -catenin, and MITF in *G9a*-amplified Hs944T cells and *G9a*-gained WM983B and K029 cells overexpressing ectopic DKK1 or GFP vector. **(I)** Effect of DKK1 overexpression on growth of *G9a*-amplified or -gained melanoma cells. Relative growth was determined by crystal violet staining 5 days after DKK1 overexpression. * $p < 0.05$, ** $p < 0.01$ by unpaired T tests of 3 replicates with the Holm-Šidák correction for multiple comparisons. **(J)** Expression of *DKK1* mRNA in pMEL*/NRAS cells 72 h after infection with GFP (control), *G9a* wild type (WT), or G1069L/W mutants. * $p < 0.05$, *** $p < 0.001$ vs. GFP control, § $p < 0.05$ vs. *G9a* WT by one-way ANOVA of 3 replicates with the Holm-Šidák correction for multiple pairwise comparisons. **(K)** Western blots for MITF expression pMEL*/NRAS 72h after infection with GFP (control), *G9a* WT, *G9a* G1069L or G1069W mutant.

Supplementary Figure S7.



Supplementary Figure S8. Correlations of *G9a* copy number/expression with WNT signatures in CCLE and with *CD8A* expression in the TCGA melanoma dataset (Related to Figure 5).

(A) Correlations of WNT signature scores

[WNT_BETA_CATENIN_UP_MELANOMA (GSE32907)] with *G9a* copy number variations and somatic missense/nonsense mutations within WNT/ β -catenin pathways (β -catenin destruction complex) in CCLE melanoma cell lines. The WNT signature scores were calculated by ssGSEA (Barbie DA et al, Nature, 2009) using the CCLE microarray dataset. Melanoma cell lines were classified according to the WNT signature scores and genetic alterations of β -catenin destruction component genes using hierarchical clustering with the one minus Pearson correlation column distance metric and complete linkage method.

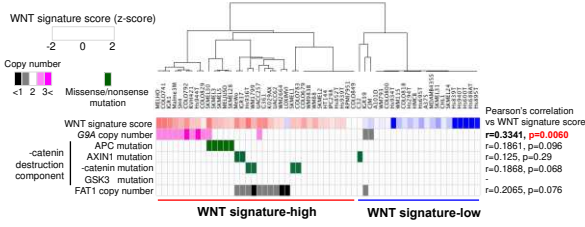
Correlations between the WNT signature scores and genetic changes of each given gene were calculated using the method of Pearson (GENE-E). **(B)** Mutual exclusivity of *G9a* copy number gain with genetic alterations in β -catenin destruction complex genes (*APC*, *AXIN1*, *β -catenin*, *GSK3 β* and *FAT1*) in high-WNT signature melanoma cell lines. Contingency of the mutual exclusivity was analyzed statistically by the Fisher exact test. **(C)** Colorimetric chart shows

significant correlations between *G9a* mRNA expression and WNT target gene signatures in melanoma and non-melanoma cancer cell line panels (CCLE and Lin et al, *Cancer Res.* **68**, 664-673, 2008). Statistical significance was determined by GSEA ($p < 0.05$, $FDR < 0.25$). **(D)** CCLE cancer types with significant positive correlations between *G9a* expression and WNT target

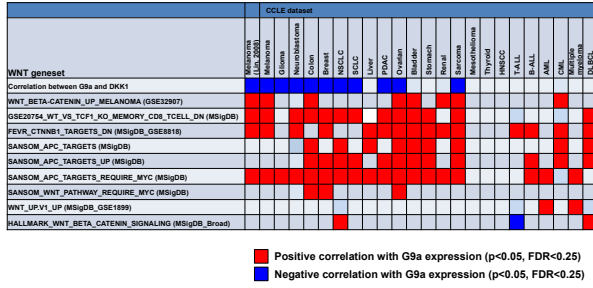
signature gene sets, SANSOM_APC_TARGET_REQUIRE_MYC (MSigDB, Broad), but no significant correlation between *G9a* and *DKK1*. **(E)** The expression levels of T-cell signature genes and *G9a* copy numbers in TCGA melanomas were obtained from cBioportal (<http://www.cbioportal.org>). The expression data were stratified according to the *G9a* copy number and plotted. Diploid vs. gain groups were compared by unpaired, two-tailed T-test.

Supplementary Figure S8.

A



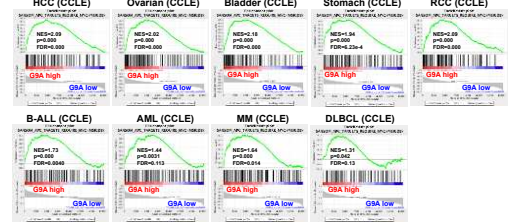
C



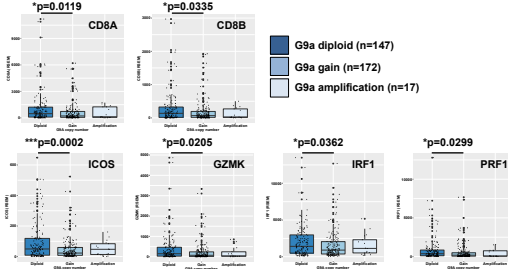
B

WNT signature	a) G9a copy number	b) Genetic changes in WNT pathway	# of cases				Log Odds Ratio	Tendency	P ₀ value
			Neither	a not b	b not a	Both			
High	G9a gain or amplification	APC/AXIN1/-catenin/FAT1 mutation or deletion	10	9	16	2	-2.768	Mutual exclusivity	0.0293
Low	G9a gain or amplification	APC/AXIN1/-catenin/FAT1 mutation or deletion	20	0	2	0	-	-	1.000

D



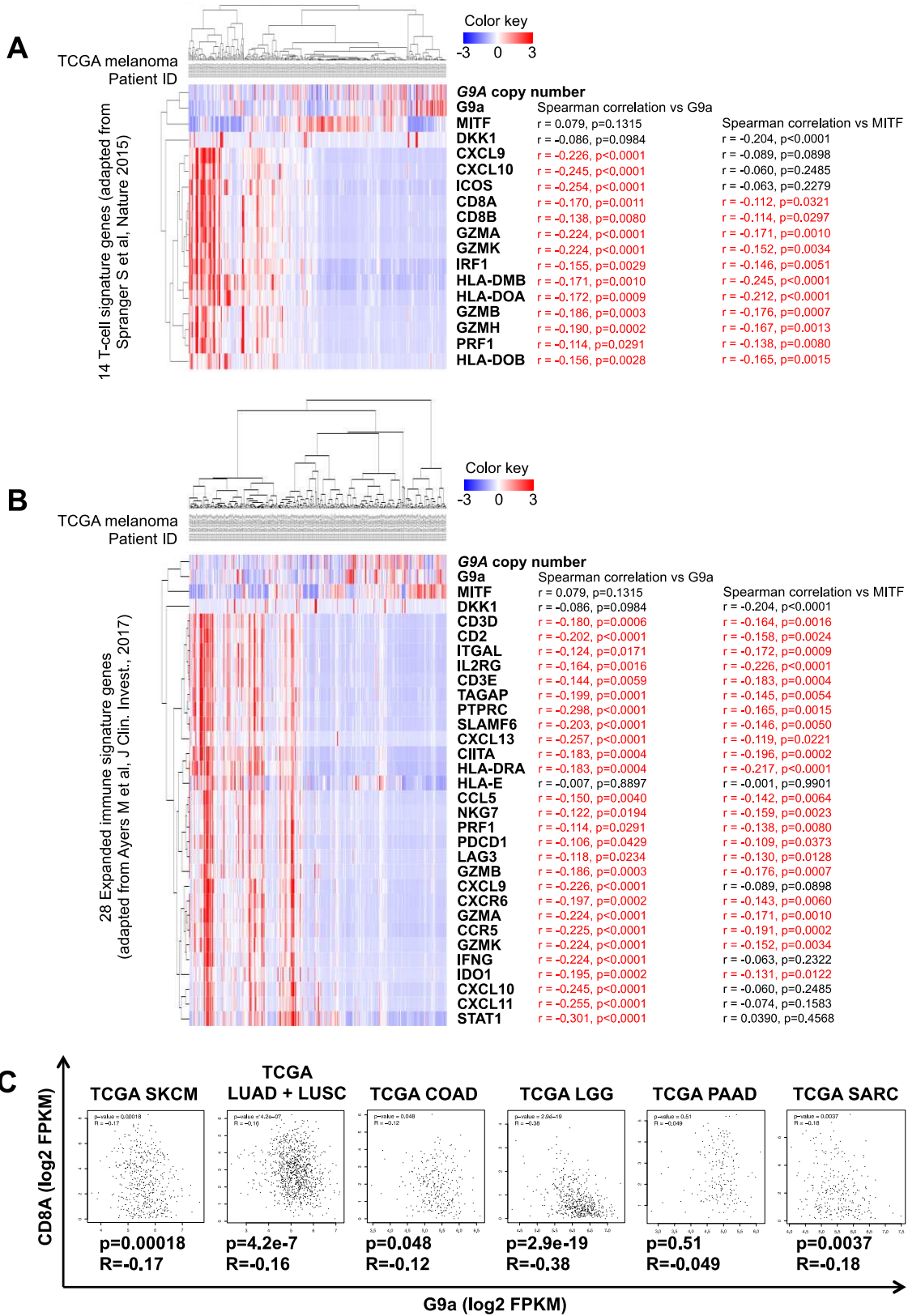
E



Supplementary Figure S9. Correlations between G9a, MITF and T-cell signature genes. (Related to Fig. 5)

(A and B) Hierarchical clustering of 367 TCGA melanoma patients with complete linkage by *G9a* copy number/expression, *MITF* expression, *DKK1* expression and Spranger T-cell signature (A) or Ayers Expanded Immune Signatures (B). Correlations between *G9a* or *MITF* expression and each T-cell signature gene were analyzed by Spearman's rank correlation. **(C)** Correlations between mRNA expression levels (FPKM) of *G9a* and *CD8A*, a marker for CD8⁺ immune populations, in various TCGA datasets. The correlations were statistically confirmed by Spearman's rank correlation.

Supplementary Figure S9.



Supplementary Figure S10. Clinical impact of *G9a* copy number gains and its association with a suppressed immune microenvironment and high WNT/ β -catenin activity. (Related to Fig. 5)

(A-D) Analysis of the Leeds Melanoma Cohort. **(A)** Scatterplot representing correlation of *G9a* mRNA expression (log₂) and *G9a* copy number (above or below diploid set at 0) (Spearman's rank correlation). The data were split into equal quartiles, with the highest quartile of *G9a* copy numbers (*G9a* high tumors) denoted by red dots and the lowest quartile (*G9a* low tumors) denoted by blue dots. **(B)** Kaplan Meier plot showing the difference in melanoma specific survival between patients harboring *G9a* low vs. *G9a* high tumors. The p-value was estimated based on the likelihood ratio test. **(C)** Stack bars showing the proportions of *G9a* low and high tumors across the six consensus immune clusters (CICs). **(D)** Volcano plot representing genes that vary significantly between *G9a* low vs. high tumors. Genes with z-scores <0 were upregulated in the *G9a* high tumors, genes with z-scores >0 were downregulated in the *G9a* high tumors. Z-scores and p-values were obtained from whole transcriptome Mann-Whitney U tests with the Benjamini-Hochberg correction for multiple testing. Pathways enriched for genes that are upregulated in *G9a* high tumors are listed in the inset; P=Panther, R=Reactome, K=KEGG. Genes highlighted in the volcano plot pertain to the WNT signaling pathway. **(E and F)** Kaplan Meier plots showing different outcomes in response to anti-CTLA-4 (E) and anti-PD-1 (F) between *G9a*-low, -med and -high melanoma patients.

Supplementary Figure S10.

